

# **Specification of the Advanced Burner Test Reactor Multi-Physics Coupling Demonstration Problem**

---

**Nuclear Engineering Division**

### **About Argonne National Laboratory**

Argonne is a U.S. Department of Energy laboratory managed by UChicago Argonne, LLC under contract DE-AC02-06CH11357. The Laboratory's main facility is outside Chicago, at 9700 South Cass Avenue, Argonne, Illinois 60439. For information about Argonne and its pioneering science and technology programs, see [www.anl.gov](http://www.anl.gov).

### **DOCUMENT AVAILABILITY**

**Online Access:** U.S. Department of Energy (DOE) reports produced after 1991 and a growing number of pre-1991 documents are available free via DOE's SciTech Connect (<http://www.osti.gov/scitech/>)

### **Reports not in digital format may be purchased by the public from the National Technical Information Service (NTIS):**

U.S. Department of Commerce  
National Technical Information Service  
5301 Shawnee Rd  
Alexandria, VA 22312

**[www.ntis.gov](http://www.ntis.gov)**

Phone: (800) 553-NTIS (6847) or (703) 605-6000

Fax: (703) 605-6900

Email: [orders@ntis.gov](mailto:orders@ntis.gov)

### **Reports not in digital format are available to DOE and DOE contractors from the Office of Scientific and Technical Information (OSTI):**

U.S. Department of Energy  
Office of Scientific and Technical Information  
P.O. Box 62  
Oak Ridge, TN 37831-0062

**[www.osti.gov](http://www.osti.gov)**

Phone: (865) 576-8401

Fax: (865) 576-5728

Email: [reports@osti.gov](mailto:reports@osti.gov)

### **Disclaimer**

This report was prepared as an account of work sponsored by an agency of the United States Government. Neither the United States Government nor any agency thereof, nor UChicago Argonne, LLC, nor any of their employees or officers, makes any warranty, express or implied, or assumes any legal liability or responsibility for the accuracy, completeness, or usefulness of any information, apparatus, product, or process disclosed, or represents that its use would not infringe privately owned rights. Reference herein to any specific commercial product, process, or service by trade name, trademark, manufacturer, or otherwise, does not necessarily constitute or imply its endorsement, recommendation, or favoring by the United States Government or any agency thereof. The views and opinions of document authors expressed herein do not necessarily state or reflect those of the United States Government or any agency thereof, Argonne National Laboratory, or UChicago Argonne, LLC.

## **Specification of the Advanced Burner Test Reactor Multi-Physics Coupling Demonstration Problem**

---

prepared by  
E. R. Shemon, J. J. Grudzinski, C. H. Lee, J.W. Thomas, and Y.Q. Yu  
Nuclear Engineering Division, Argonne National Laboratory

December 21, 2015



## ABSTRACT

This document specifies the multi-physics nuclear reactor demonstration problem using the SHARP software package developed by NEAMS. The SHARP toolset simulates the key coupled physics phenomena inside a nuclear reactor. The PROTEUS neutronics code models the neutron transport within the system, the Nek5000 computational fluid dynamics code models the fluid flow and heat transfer, and the DIABLO structural mechanics code models structural and mechanical deformation. The three codes are coupled to the MOAB mesh framework which allows feedback from neutronics, fluid mechanics, and mechanical deformation in a compatible format.

A key focus of the multi-physics coupling demonstration is to demonstrate reactivity feedback due to structural/mechanical deformation. After surveying several options, the Advanced Burner Test Reactor (ABTR) was chosen as the target demonstration problem for the following reasons: (1) the design of ABTR incorporates structural mechanical feedback by assembly bowing, and (2) information on the ABTR is readily available, unlike other facilities like the Fast Flux Test Facility.

In this document, the ABTR model is defined for the SHARP tool package multi-physics coupling demonstration. The document also presents the modeling assumptions used and key demonstration objectives.

## Table of Contents

Abstract .....	ii
Table of Contents .....	iii
List of Figures .....	iv
List of Tables.....	v
1 Introduction .....	1
2 Advanced Burner Test Reactor Plant Overview .....	1
3 Reactor Core Geometry.....	3
3.1 Fuel Assembly.....	5
3.2 Control Assembly .....	8
3.3 Reflector and Shield Assemblies .....	10
3.4 Material and Fuel Test Assemblies .....	12
4 Reactor Core Material Compositions.....	13
4.1 Fuel TRU Compositions .....	13
4.2 Material Densities .....	13
5 Structural Mechanical Specification .....	14
5.1 Core Restraint System.....	17
5.2 Core Mechanical Geometry .....	19
5.3 Structural Mechanical Material Properties.....	23
6 Thermal Hydraulic Specification .....	24
6.1 Inlet and Outlet Temperatures.....	24
6.2 Material Properties for T/H.....	25
6.3 Core Subassembly Flow Allocation and Power.....	26
7 Kinetics Parameters.....	28
References .....	29

## LIST OF FIGURES

Figure 2.1 Vertical View of Primary System.....	2
Figure 3.1 ABTR Full Core Assembly Layout.....	3
Figure 3.2 Illustration of Assembly Duct Parameters.....	4
Figure 3.3 Fuel Assembly Schematic (Hot Condition).....	6
Figure 3.4 Fuel Pin Diagram (Cold Condition). ....	7
Figure 3.5 Control Assembly Absorber Region Containing Two Ducts .....	8
Figure 3.6 Control Assembly Schematic (Hot Condition).....	10
Figure 3.7 Radial Reflector/Shield Assembly Schematic (Hot Condition) .....	12
Figure 5.1 Illustration of a Typical Sodium-Cooled Fast Reactor Fuel Assembly.....	14
Figure 5.2 Schematic of Core Geometry with Core Support and Restraint System Context. .	15
Figure 5.3 Schematic of Lower Internal Structure.....	16
Figure 5.4 Cross section of Reactor Vessel Showing Core Barrel and Restraint System Location.....	16
Figure 5.5 Schematic of Limited Free Bow Core Restraint System Components and Key Dimensions.....	18
Figure 5.6 Illustration of Limited Free Bow Core Restraint Concept.....	18
Figure 5.7 Schematic for Duct Dimensions. ....	19
Figure 5.8 Schematic of Restraint Ring Gap Dimensions at TLP which illustrates the Load Pad Gap (R) and the Load Pad-TLP Restraint Ring gap (Q).....	20
Figure 5.9 Plan View of Typical Restraint Ring.....	20
Figure 5.10 Core Restraint Schematic for Dimensions Showing Top Load Pad (TLP) and Above Core Load Pad (ACLP). ....	21
Figure 5.11 Dimensions for Core Barrel.....	21
Figure 5.12 Additional Detail of Duct Inlet Nozzle Connection to Inlet Receptacle. ....	22
Figure 5.13 Illustration of Duct Boundary Condition: Nozzle Laterally Restrained by Contact with Receptacle. ....	22
Figure 6.1 Subchannel Assignments in Safety Analysis Model [7].....	26
Figure 6.2 Initial Subassembly Flow Rate (kg/s) in Safety Analysis Model [7] .....	27
Figure 6.3 BOEC Subassembly Powers (MW) [7]. ....	27

## LIST OF TABLES

Table 2.1 ABTR Plant Design Parameters.....	2
Table 3.1 Assembly Duct Geometry Parameters .....	4
Table 3.2 Thermal Expansion Data at Operating Condition.....	4
Table 3.3 Fuel Assembly Axial Description .....	5
Table 3.4 Fuel Assembly Parameters.....	7
Table 3.5 Control Assembly Axial Description (Rods Out).....	9
Table 3.6 Control Assembly Geometry Parameters.....	9
Table 3.7 Reflector and Shield Assembly Axial Description .....	11
Table 3.8 Reflector Assembly Geometry Parameters .....	11
Table 3.9 Shield Assembly Geometry Parameters.....	11
Table 4.1 Fuel TRU Fractions.....	13
Table 4.2 Basic Material Assignments, Density and Atomic Fractions. ....	13
Table 5.1. Key Dimensions Related to the Core Restraint Design Shown in Figure 5.7 through Figure 5.12 (Evaluated at $T_{ref} = 21^{\circ}\text{C}$ ).....	23
Table 5.2 Component Materials.....	24
Table 5.3 Mechanical Properties for HT-9. ....	24
Table 6.1 Assumed Temperature at Operating Condition .....	25
Table 6.2 Thermal Hydraulic Properties for Materials .....	25
Table 6.3 Flow Allocation in Safety Analysis Model [7] .....	26
Table 7.1 Kinetics Parameters and Reactivity Coefficients (from Ref. [7]).....	28

## 1 Introduction

The purpose of this document is to specify the multi-physics nuclear reactor demonstration problem which will be performed for the DOE-NE Advanced Reactor Concepts (ARC) program using the SHARP software package [1] developed by the DOE-NE Nuclear Energy Advanced Modeling (NEAMS) and Simulation program.

The SHARP toolset simulates the key physics phenomena inside a nuclear reactor using a trio of individual physics codes which provide power, temperature, density, and structural feedback. PROTEUS [2] models the neutron transport within the system, Nek5000 [3] models computational fluid dynamics, and DIABLO [4] models structural and mechanical deformation. The three codes are loosely coupled via the MOAB [5] mesh framework which facilitates communication between the neutronics, fluid mechanics, and mechanical deformation modules.

A key focus of the multi-physics coupling demonstration is to demonstrate reactivity feedback due to structural mechanical deformation. After surveying several options, the Advanced Burner Test Reactor (ABTR) was chosen as the target demonstration problem for the following reasons: (1) the design of ABTR incorporates structural mechanical feedback by assembly bowing, and (2) information on the ABTR is readily available, unlike some other facilities. While much of the ABTR design has previously been published, reasonable inferences have been made for missing characteristics such as the core inlet plenum geometry.

In this document, the ABTR model is defined for the NEAMS/SHARP tool package multi-physics coupling demonstration. The document also presents the modeling assumptions used and key demonstration objectives. We note that the majority of the technical content and figures presented here are a condensation of content and figures available in previously published reports, referenced as applicable.

## 2 Advanced Burner Test Reactor Plant Overview

The Advanced Burner Test Reactor (ABTR) is a conceptual advanced sodium-cooled nuclear reactor designed by Argonne National Laboratory [6,7]. ABTR is rated for a thermal power of 250 MW with an electric output of approximately 95 MW (38% thermal efficiency). The reactor core contains 199 assemblies, including 54 driver fuel assemblies [7]. The 24 inner zone and 30 outer zone fuel assemblies differ only in their TRU enrichment. The reference fuel design uses weapons-grade plutonium-based ternary metal (U-TRU-10Zr). There are 7 primary and 3 secondary control rod assemblies for providing reactivity control. In addition, 9 test assembly locations are provided (six for fuel tests and three for material tests).

All primary system components are submerged in a sodium pool-type configuration as illustrated in Figure 2.1, which shows the elevation view of the primary system. The sodium coolant inlet and outlet temperatures are 355°C and 510°C, respectively. The cold pool level is 10.16 m above the bottom of the pressure vessel. The hot pool level is at 12.20 m elevation above the bottom of the pressure vessel (2.04 m above the cold pool level).

Major plant design parameters are summarized in Table 2.1.

**Table 2.1 ABTR Plant Design Parameters**

Reactor Power	250 MWt, 95 MWe
Coolant	Sodium
Coolant Temperature, Inlet/Outlet	355°C / 510°C
Driver Fuel	U-TRU-10Zr (~20% TRU, 80% U) with WG-Pu TRU feed
Cladding and Duct Material	HT-9
Cycle Length	4 months
Plant Life	30 years with expectation of life extension
Reactor Vessel Size	5.8 m diameter, 16 m height
Structural and Piping Material	Austenitic Stainless Steel
Primary Pump	Reference: Electromagnetic Backup: Mechanical (centrifugal)
Power Conversion Cycle	Supercritical CO2 Brayton
Thermal Efficiency	38%

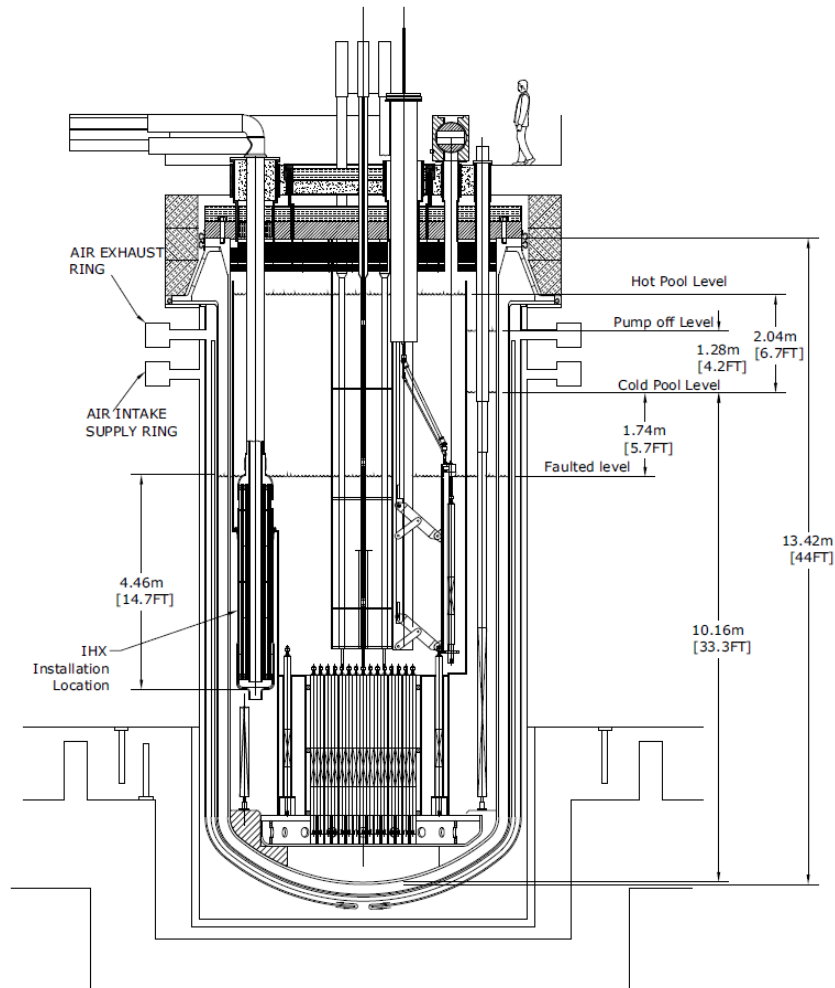


**Figure 2.1 Vertical View of Primary System.**

Details regarding the reactor geometry, materials, neutronics, thermal hydraulics, and structural mechanics properties are given in the following sections.

### 3 Reactor Core Geometry

The core assembly layout of the 250 MWt ABTR reference design is illustrated in Figure 3.1 [7]. The 199 assemblies can be categorized and counted as 54 driver fuel assemblies, 78 reflector assemblies, 48 shield assemblies, 10 control rod assemblies, and 6 fuel test assemblies, and 3 material test assemblies. The assemblies are laid out in a regular hexagonal lattice. The core barrel inner diameter is 2.27 m, and the equivalent core outer diameter is 1.31 m.

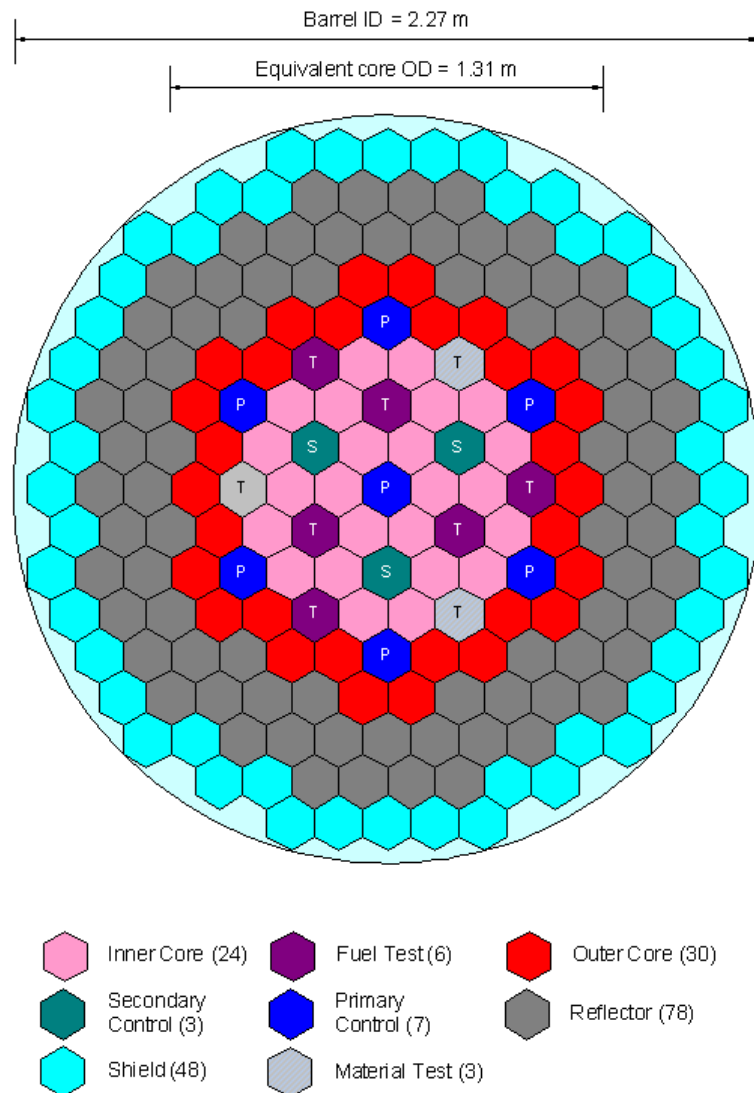


**Figure 3.1 ABTR Full Core Assembly Layout**

The 54 driver fuel assemblies are categorized into 24 inner zone driver assemblies and 30 outer zone driver assemblies. The inner zone driver assemblies have lower TRU enrichment (16.5%) than the outer zone assembly (20.7%) which helps to maintain a flattened power distribution.

All ABTR assemblies have the same HT-9 hexagonal duct structure, SS-316 lower structure, and upper handling socket. Sodium flows through the gaps between assemblies. The general dimensions of the assembly duct are given in Table 3.1 for both cold and hot (operating) conditions. The hot conditions were derived using the thermal expansion factors in Table 3.2.

**Table 3.1 Assembly Duct Geometry Parameters**

	<b>Cold</b>	<b>Hot</b>
Duct Material	HT-9	HT-9
Total length of duct, cm	328.000	329.604
Assembly pitch, cm	14.5980	14.6850
Duct outer flat-to-flat distance, cm	14.1980	14.2826
Duct wall thickness, cm	0.3000	0.3018
Duct inside flat-to-flat distance, cm	13.5980	13.6790
Inter-assembly gap, cm	0.4000	0.4024*

\* Inferred from hot assembly pitch and hot duct outer flat-to-flat distance

**Table 3.2 Thermal Expansion Data at Operating Condition**

Radial Expansion Factor $\alpha_r$	0.596%
Axial Expansion Factor $\alpha_a$	0.489%
Fuel Axial Swelling Factor $\alpha_s$	5.000%
Axial expansion of control rod absorber	0.540%

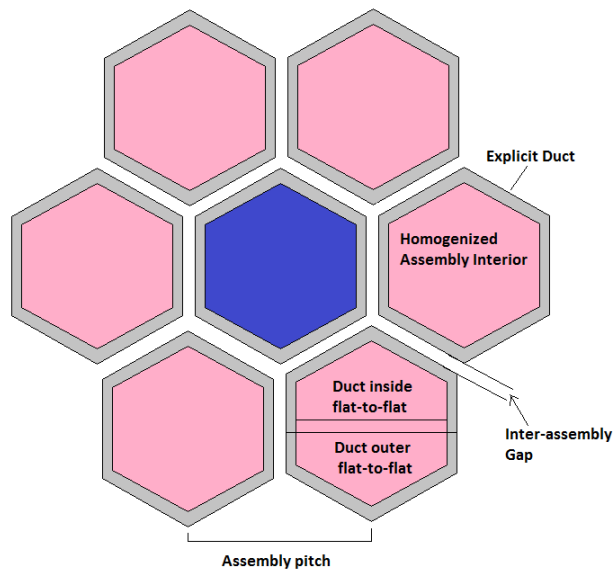


**Figure 3.2 Illustration of Assembly Duct Parameters.**

Figure 3.2 illustrates the duct parameters given in Table 3.1 and the explicit form of the duct which will be modeled in this demonstration. Detailed descriptions for the individual assembly types are given in the following sections. We note that the cold condition length of the duct is taken from Ref. [7] and the hot condition length is taken by multiplying by the axial expansion coefficient.

### 3.1 Fuel Assembly

The axial regions of the fuel assembly are described in Table 3.3 and shown in Figure 3.4. The lowest axial region (near the cold sodium inlet) is a structural nosepiece made of SS-316. We note the structural nosepiece length was assumed to be 38.0 cm (cold condition) [7] versus the value of 50.0 cm appearing other unpublished analysis reports. For homogenization purposes, the nosepiece is assumed to occupy 30% of the volume with sodium coolant occupying the other 70%.

Just beneath the active core is a lower shield (reflector) containing solid HT-9 rods for shielding. The shield is an integral part of the fuel pin in the form of an extended fuel-pin bottom end cap.

The active core containing the fissionable material is located above the lower shield (reflector). The active core geometry will be described momentarily. The upper gas plenum above the active core serves to contain fission gases released during operation. At hot conditions, the upper gas plenum is also partially filled with displaced sodium bond. The uppermost axial region is the handling socket or “upper structure”.

**Table 3.3 Fuel Assembly Axial Description**

Axial Region	Material(s)	Region Length (cm)		Height Relative to Bottom of Assembly (cm)	
		Cold	Hot	Cold	Hot
Handling Socket (Upper Structure)	SS-316 with sodium coolant	30.00	30.15	328.00	329.604
Upper Gas Plenum (no sodium bond)	HT-9 clad, fission gas, sodium coolant	120.00	96.80	298.00	299.454
Upper Gas Plenum (with sodium bond)	HT-9 clad, sodium bond, sodium coolant	0.00	19.764	178.00	202.654
Active Core	HT-9 clad, fuel slugs, sodium bond (cold), sodium coolant	80.00	84.411	178.00	182.89
Lower Reflector	solid HT-9 rods, sodium coolant	60.00	60.293	98.00	98.479
Nosepiece (Lower Structure)	SS-316 with sodium coolant	38.00	38.186	38.00	38.186

The active core region consists of 217 fuel pins arranged in a 9-ring hexagonal lattice. Each fuel pin is an HT-9 clad tube containing a central stack of fuel pellets and a filler of sodium bond in the fuel-clad gap. At hot condition, the fuel pellet thermally expands and displaces the sodium bond into the upper gas plenum. Sealed-type pins are used to contain the fuel and fission products. Each fuel pin is helically wrapped with wire to maintain the pin spacing such that coolant can flow freely through the pin bundle. Both cold and hot dimensions of the fuel pins are listed in Table 3.4.

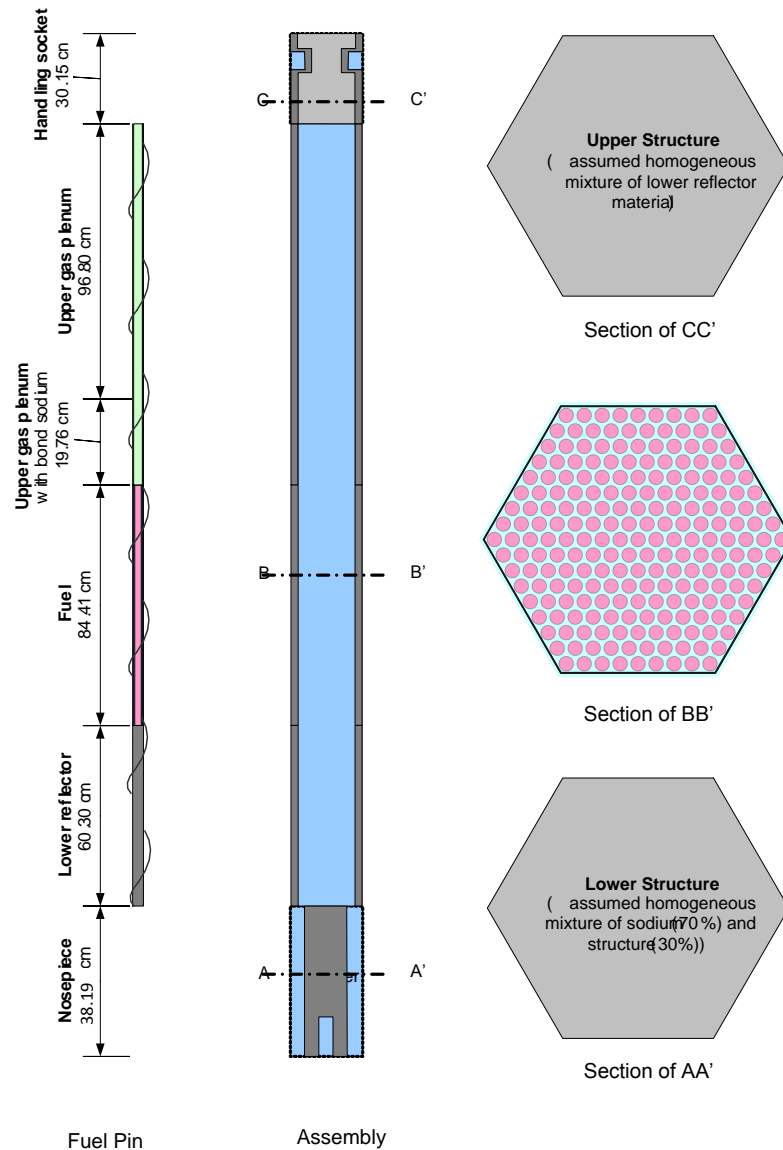


**Figure 3.3 Fuel Assembly Schematic (Hot Condition).**

As previously mentioned, the 54 fuel assemblies are divided into 24 inner core assemblies and 30 outer core assemblies with fuel enrichments (i.e. TRU fractions) of 16.5% and 20.7%, respectively. Fuel assembly parameters and a schematic for the fuel pin are given in Table 3.4 and

Figure 3.3, respectively. The fuel assembly parameters apply to the active core region, lower reflector, and upper gas plenum regions which all have the same pin geometry. *We note that the fuel assembly volume fractions were taken from Table 3.4 and correspond to a completely homogenized assembly geometry (duct homogenized as well).*

**Table 3.4 Fuel Assembly Parameters**

	<b>Cold</b>	<b>Hot</b>
Number of pins	217	217
Fuel pin smear density, %	75	100
Fuel pin pitch, cm	0.9080	0.9134
Outer radius of clad, cm	0.4000	0.4024
Inner radius of clad, cm	0.3480	0.3501
Fuel slug radius, cm	0.3014	0.3501
Wire wrap radius, cm	0.0515	0.0518
Wire wrap axial pitch, cm	20.3200	21.4404
Smear clad outer radius with wire-wrap, cm (for case of explicit wire wrap modeling)		0.4057
Volume fractions (includes homogenization of duct) <sup>1</sup>		
- Fuel	0.3355	0.3142
- Clad	0.1536	0.1510
- Duct	0.0783	0.0770
- Sodium bond	0.1118	0.0000
- Coolant	0.3208	0.3208

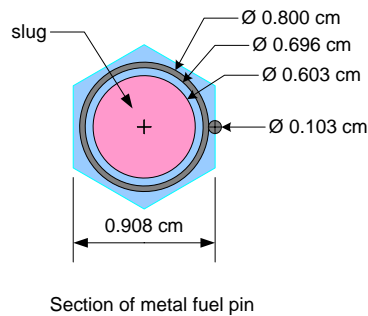


**Figure 3.4 Fuel Pin Diagram (Cold Condition).**

<sup>1</sup> The volume fractions in this table and similar tables were calculated for previous REBUS-3/DIF3D inputs. The hot volume fractions were calculated to preserve the same mass at the hot condition using the number densities at the cold conditions. The ratio of the sums between the cold and hot conditions should be the same as the reverse ratio of the two volumes. The volume fractions listed here also include the homogenized duct which is not the model for the ARC problem.

### 3.2 Control Assembly

The ABTR employs two independent reactivity control systems. The primary control system consists of one central control assembly and an additional six control assemblies placed in the fifth ring. The secondary control system consists of three control assemblies placed in the third ring.

In addition to the main outer duct, the control assemblies have a second interior duct. The interior duct is stationary and runs from the lower to upper portion of the core. An absorber bundle consisting of 91 absorber pins slides up and down within the interior duct. The absorber pins contain compacted boron carbide pellets. All pins in a single control assembly move together. Sealed-type pins are used to contain reaction byproducts. A channel of sodium runs between the inner and outer duct.

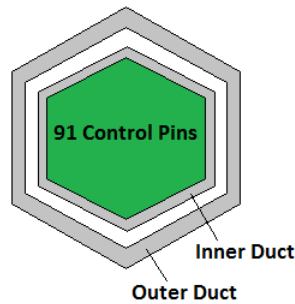


**Figure 3.5 Control Assembly Absorber Region Containing Two Ducts**

Each control assembly contains the following axial regions from bottom to top: lower structure (mixture of sodium and structural material), lower reflector, empty region (sodium and structure), follower, absorber, upper gas plenum, and upper structure. The lower and upper structures are similar to the fuel assembly, except that the lower structure (nosepiece) has unique features to preclude inadvertent installation into an unassigned core position. The follower region contains a central, solid SS-316 rod of radius 5.00 cm surrounded by sodium coolant. The absorber region contains the control material. The absorber and upper gas plenum regions are helically wrapped with wire similar to the fuel assembly. The control assembly axial description in Table 3.5 corresponds to the case where the control rods are positioned above the active core. Note that the top of the active core region is at axial height 182.89 cm which is below the bottom of the absorber region in the control assembly.

**Table 3.5 Control Assembly Axial Description (Rods Out).**

Axial Region	Material(s)	Region Length (cm)		Height Relative to Bottom of Assembly (cm)	
		Cold	Hot	Cold	Hot
Handling Socket (Upper Structure)	SS-316 with sodium coolant	30.00	30.15	328.00	329.604
Upper gas plenum	HT-9 Clad, Gas, Sodium Coolant	31.00*	31.14	298.00	299.4539
Absorber	HT-9 Clad, B <sub>4</sub> C pellets, Sodium coolant	85.00	85.4157	267.00	268.3139
Follower	SS-316 Rod, Sodium coolant	16.80	16.8822	182.00	182.8982
Empty Duct	Sodium	85.10*	85.51	165.20	166.016
Lower Reflector	HT-9 and sodium (similar to fuel assembly lower reflector)	42.10*	42.32	80.10	80.506
Nosepiece (Lower Structure)	SS-316 with sodium coolant	38.00	38.186	38.00	38.186

\* inferred from thermal expansion data

**Table 3.6 Control Assembly Geometry Parameters**

	Cold	Hot
Number of pins	91	91
Rod pitch	1.2484	1.2558
Absorber smeared density, %	85	85
Thickness of clad, cm	0.0700	0.0704
Outer radius of clad, cm	0.5552	0.5585
Inner radius of clad, cm	0.4852	0.4881
Absorber radius, cm	0.4473	0.4881
Inner duct outer flat-to-flat distance, cm	12.7980	12.8743
Inner duct inner flat-to-flat distance, cm	12.1980	12.2707
Wire wrap radius, cm	0.0665	
Wire wrap axial pitch, cm	20.3200	21.4404
Clad outer radius with wire-wrap		0.5626
Radius of follower	5.0000	5.0298
Volume fraction (includes homogenization of duct)		
- Absorber	0.30996	0.30481
- Clad	0.11979	0.11780
- Duct	0.14864	0.14617
- He bond	0.05470	0.00000
- Coolant	0.36691	0.36692

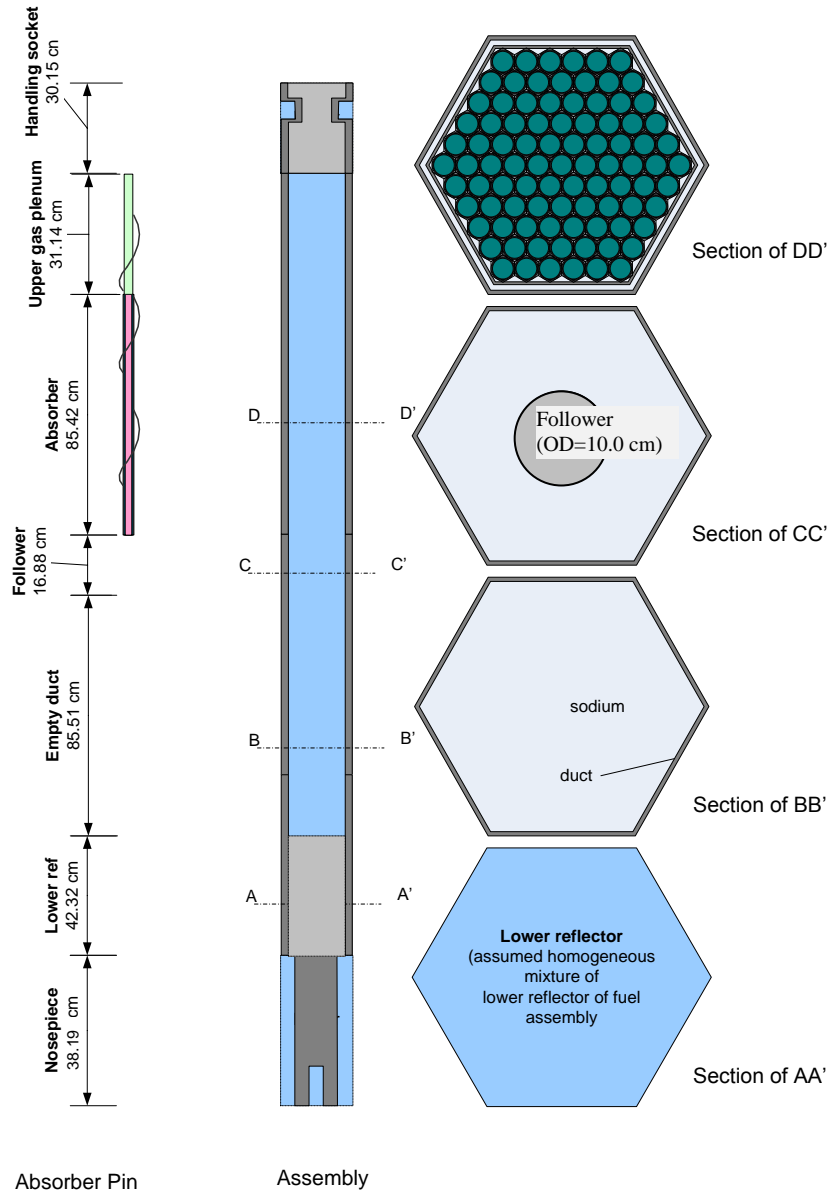


**Figure 3.6 Control Assembly Schematic (Hot Condition)**

### 3.3 Reflector and Shield Assemblies

Each of the 78 reflector assemblies contains a bundle of 91 solid HT-9 rods arranged in 6 concentric hexagonal rings. The HT-9 pin volume fraction is 75.2% and the duct volume fraction is 7.7 %, yielding the total HT-9 volume fraction of 83.9% at the operating condition in the assembly-homogenized case.

The reflector and shield assemblies have the simplest axial geometry. Each reflector and shield assembly contains the following axial regions from bottom to top: lower structure, reflector or shield, and upper structure.

**Table 3.7 Reflector and Shield Assembly Axial Description**

Axial Region	Material(s)	Region Length (cm)		Height Relative to Bottom of Assembly (cm)	
		Cold	Hot	Cold	Hot
Handling Socket (Upper Structure)	SS-316 with sodium coolant	30.00	30.15	328.00	329.607
Reflector or Shield	Solid HT-9 Rods (Reflector) or HT-9-clad B <sub>4</sub> C pins (Shield), sodium coolant	260.00	261.271	298.00	299.457
Nosepiece (Lower Structure)	SS-316 with sodium coolant	38.00	38.186	38.00	38.186

**Table 3.8 Reflector Assembly Geometry Parameters**

	Cold	Hot
Number of pins	91	91
Pin pitch, cm	1.4067	1.4151
Reflector rod radius, cm	0.7026	0.7068
Volume fraction (includes homogenization of duct)		
- Reflector	0.76470	0.75199
- Duct	0.07826	0.07696
- Coolant	0.15704	0.15704

Each of the 48 shield assemblies contains 19 thick HT-9 tubes containing B<sub>4</sub>C (boron carbide) absorber pellets. Natural boron (B-10 abundance of 19.9 atomic percent) is used with 81% smeared B<sub>4</sub>C pellet density (volume fraction of the boron carbide inside the cladding). The tubes are arranged in a hexagonal lattice of 3 rings. Sealed-type pins are used to contain the absorber materials.

**Table 3.9 Shield Assembly Geometry Parameters**

	Cold	Hot
Number of pins	19	19
Shield pin pitch, cm	3.0441	3.0622
Absorber smeared density, %	81	81
Thickness of clad, cm	0.2500	0.2515
Outer radius of clad, cm	1.5213	1.5304
Inner radius of clad, cm	1.2713	1.2789
Absorber radius, cm	1.1442	1.2789
Volume fraction (includes homogenization of duct)		
- Shield	0.42341	0.41637
- Clad	0.22580	0.22050
- Duct	0.07826	0.07696
- He bond	0.09932	0.00000
- Coolant	0.17320	0.17320

The schematic for the reflector and shield assemblies is shown in Figure 3.7.

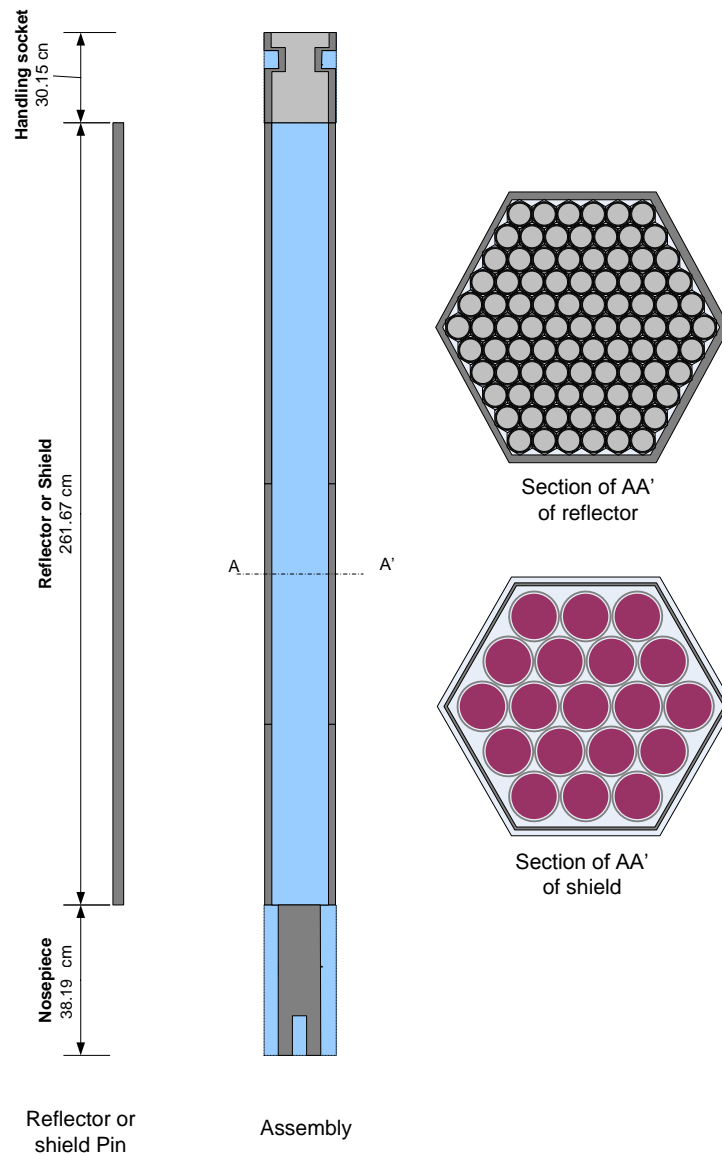


**Figure 3.7 Radial Reflector/Shield Assembly Schematic (Hot Condition)**

### **3.4 Material and Fuel Test Assemblies**

The nine test assembly locations were included to increase the flexibility of core loading and the space for irradiation test. Three assemblies located in the fourth ring are designated for material test assemblies, and six fuel test assemblies located in the third and fourth rings are designated for fuel test assemblies. Since the compositions of the test assemblies are not determined, material test assembly locations can be assumed to be loaded by reflector assemblies, and the fuel test assembly locations can be assumed to be loaded by fuel assemblies which use LWR spent fuel as the TRU source [7]. We assume the TRU fraction of heavy metal in the LWR spent fuel to be 18.68%. The TRU compositions are presented in the next section.

## 4 Reactor Core Material Compositions

### 4.1 Fuel TRU Compositions

Weapons grade Pu (WG-Pu) is used as the feed for the driver fuel U-TRU-10Zr. LWR spent fuel TRU is used as the feed for the test fuel assemblies. The two TRU compositions are not included in this report. The LWR-SF TRU compositions were determined from 10-year cooled LWR spent fuel with 33 MWd/kg burnup [7].

**Table 4.1 Fuel TRU Fractions.**

Assembly Type	% TRU fraction in Heavy Metal
Inner Core	16.53%
Fuel Test Assembly	18.68%
Outer Core	20.66%

### 4.2 Material Densities

This section describes the four major materials (sodium coolant, HT-9 clad/duct, SS-316 structural material, and the fuel slug) which are contained in this benchmark problem.

**Table 4.2 Basic Material Assignments, Density and Atomic Fractions.**

Geometry	Material	Density, g/cc	Atomic Fractions	
Coolant	Sodium	0.850257	Na	100.00%
Clad, Duct	HT-9	7.76	Fe Ni Cr Mn55 Mo	*
Grid Plate	SS-316	7.97	Fe Ni Cr Mn55 Mo	68.09% 13.98% 13.88% 2.18% 1.87%
Fuel Slug	U-TRU-10Zr	15.73	*% Zr by mass See above tables for % TRU and TRU compositions	

\*These values are not open literature

The homogenized number densities were computed based on a complete assembly homogenization (duct, fuel, and surrounding sodium in between assemblies). We wish to model the duct and sodium between ducts explicitly, so these homogenized numbers do not apply to our model. We must create new homogenized nuclide densities which exclude the duct and outer sodium.

## 5 Structural Mechanical Specification

The reactivity of a fast reactor core is sensitive to core assembly movement. Temperature changes within the reactor affect the reactivity by thermal expansion, which changes the geometry of the reactor and the density of the material within it. In addition, structural deformations affecting reactivity can be induced by temperature gradients that result in bowing, by elastic deformation due to high stresses, or by buckling as a consequence of axial restraint on thermal expansion.

To design an inherently safe fast reactor, reactivity due to bowing must be engineered into the reactor plant to assure a net negative reactivity insertion during transient events. The location and geometry of the fuel assemblies is a driving parameter for this. The reactivity of the core is very much a function of the position of the fuel elements which are supported in an array within a thin-wall hexagonal duct as illustrated in Figure 5.1 [9]. It is assumed that the fuel elements represent negligible stiffness in the fuel assembly compared to the ducts such that the ducts determine the location of the fuel. Thermal and fast neutron flux gradients within the core cause the assembly ducts to swell and bow. This bowing is both of a transient (elastic thermal strains depending upon power profile) and permanent (inelastic irradiation creep and swelling strains that depend on time and fluence) nature. Transient bowing of core assemblies causes significant changes in reactivity during reactor start-up, transient overpower (TOP), and unprotected loss of flow without scram (ULOF). During unprotected loss-of-flow (ULOF), the power over flow (P/F) ratio can reach double that of nominal conditions. The negative reactivity feedback due to bowing is usually the dominant reactivity feedback during unprotected accidents in advanced liquid metal-cooled fast reactors [10]. The permanent bowing of the ducts changes the reactivity over time and more importantly affects the mechanical forces required to refuel the core because the bowing is greater than the duct-to-duct clearance.

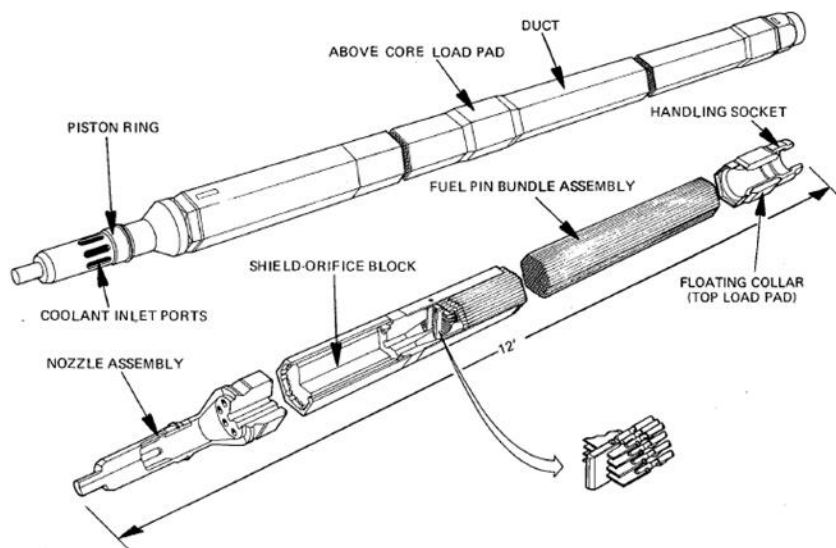


**Figure 5.1 Illustration of a Typical Sodium-Cooled Fast Reactor Fuel Assembly.**

For both safety and operational reasons, it is important to control the location of the ducts to a small tolerance. A core restraint system that properly constrains the duct location is necessary. However, it is also necessary that this system leaves a gap between ducts to accommodate irradiation swelling that accumulates over time as a result of the fast neutron fluence. If insufficient clearance exists, the ducts swell into contact with each other and become difficult to remove. The burn-up of the core is then limited by swelling. However, leaving the ducts with too much clearance provides too large of an available reactivity insertion in the event of sudden compaction.

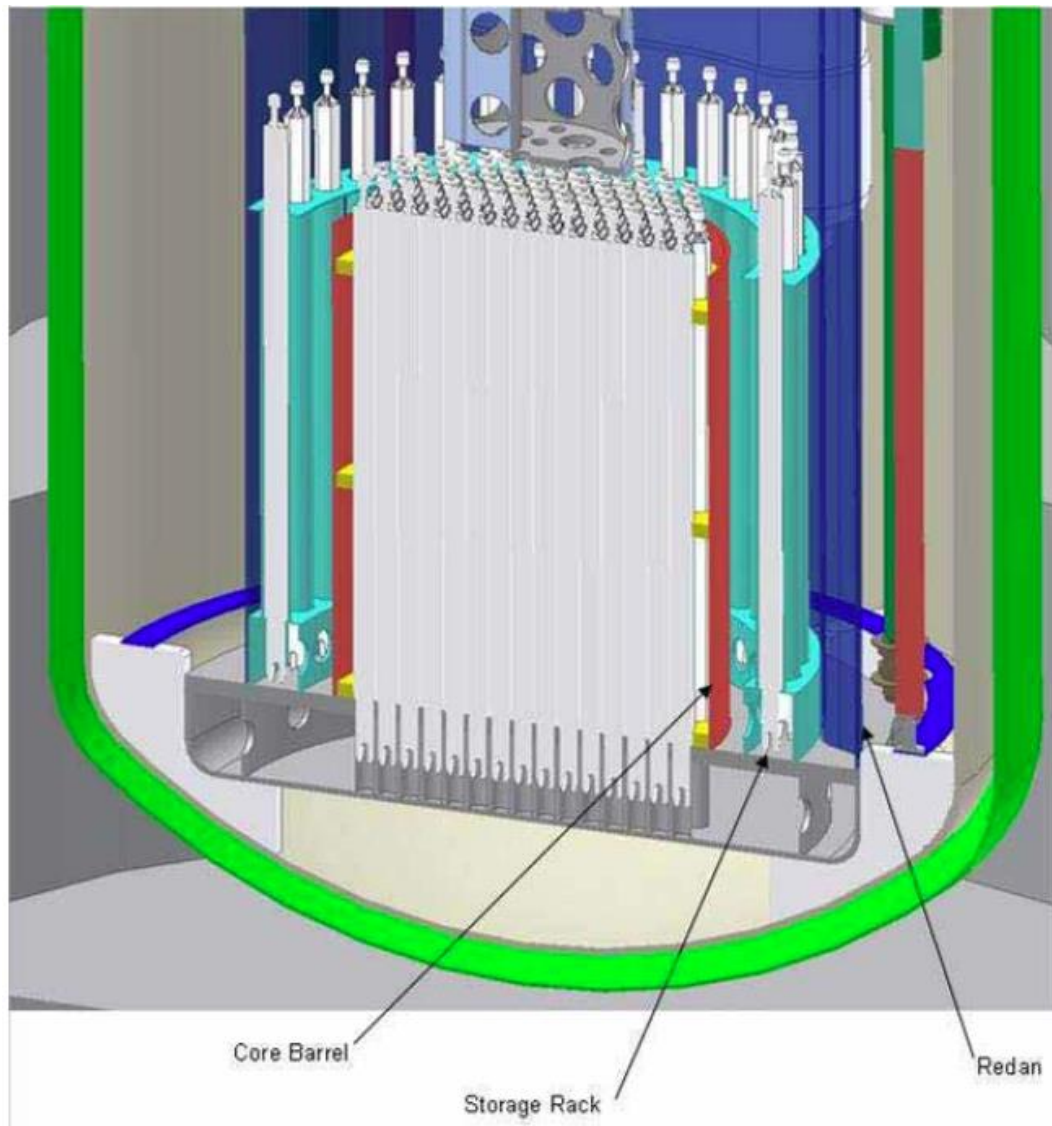


**Figure 5.2 Schematic of Core Geometry with Core Support and Restraint System Context.**

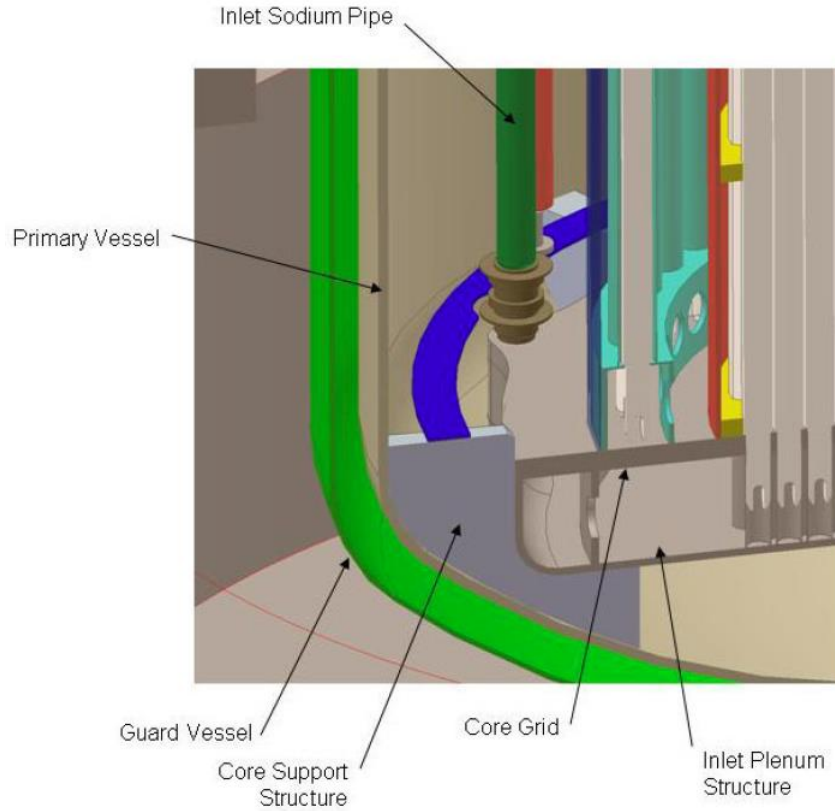


**Figure 5.3 Schematic of Lower Internal Structure.**

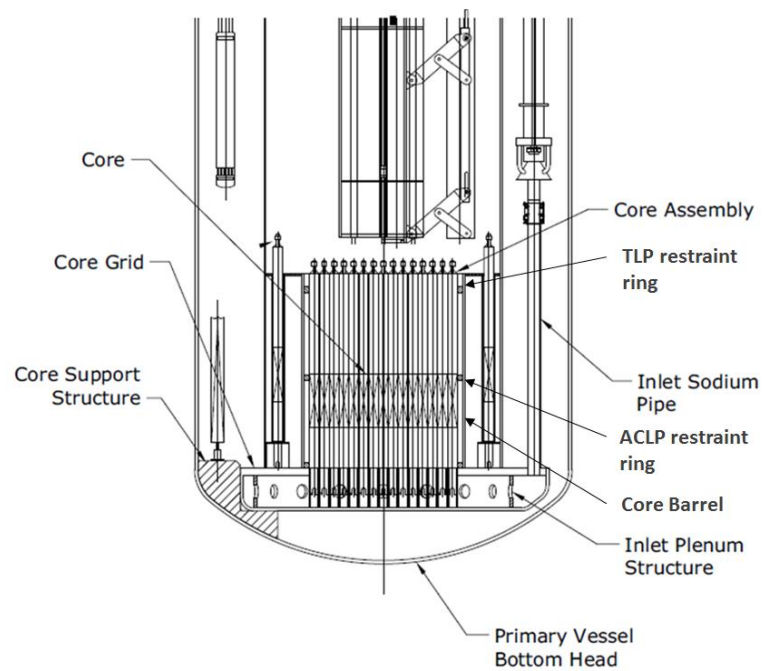


**Figure 5.4 Cross section of Reactor Vessel Showing Core Barrel and Restraint System Location.**

Figure 5.2 is an illustration of the ABTR core geometry which shows the core in the context of the core support and restraint systems. Figure 5.3 illustrates the ABTR lower internal structure including the core grid structure, core support structure, and inlet plenum structure. Parts of the the restraint system depicted in Figure 5.4 are described in the following section.

### **5.1 Core Restraint System**

The ABTR utilizes the “limited free bow” core restraint system shown in Figure 5.4 and Figure 5.5. The limited free bow restraint system is characterized by load pads on the ducts at the top (TLP) and in the region above the core (ACLP), along with restraining rings at the TLP and ACLP axial heights. The rigid restraint rings are attached to the core barrel at the ACLP and TLP locations.

The load pads serve as preferential contact points between the ducts. The load pads add only marginal thickness to the main duct body (this is exaggerated for clarity in the figure) but they are nonetheless thick enough to maintain the desired form under the design loadings. Additionally, the design ensures that duct-to-duct loading (resulting from bowed ducts in contact) is kept within allowable limits including the time-dependent inelastic bowing effects due to irradiation (and thermal) creep and swelling effects. This inelastic bowing leaves residual contact forces in the ducts at refueling temperatures which, when considered with friction effects, create additional loading during refueling. The allowable refueling loads provide a further constraint on the load pad design. The reactivity response and resulting forces on the load pads are dependent on many system variables. Many of these variables are fixed from the point of view of restraint design, (core size, pitch, temperature and flux inputs, etc.). The tunable variables of the core restraint include elevation of the load pads, clearances between the individual load pads, and clearance between the TLP restraint ring. These tunable parameters are key factors that drive the performance of the system. The parameters are shown in Figure 5.5.

The core barrel is a right circular cylinder fabricated from stainless steel. It is attached to the inlet plenum and lower support structure. The TLP clearance is small which allows only a limited amount of outward bow (flowering) before contact is made. The ACLP clearance is designed to be just large enough that contact is never made during normal reactor operations. The ACLP’s purpose is to provide a limit of motion (and hence reactivity insertion) in the event of a seismic event. An additional important feature of the limited free bow core restraint design is a nozzle connection that allows rotational freedom similar to a pinned connection.

The limited free bow core restraint system is designed to provide inherent protection against over power events by taking advantage of thermally induced bending action of the fuel ducts. This is illustrated in Figure 5.6 which shows a row of three cantilevered ducts located symmetrically about the center of a core and in a radially varying thermal gradient.

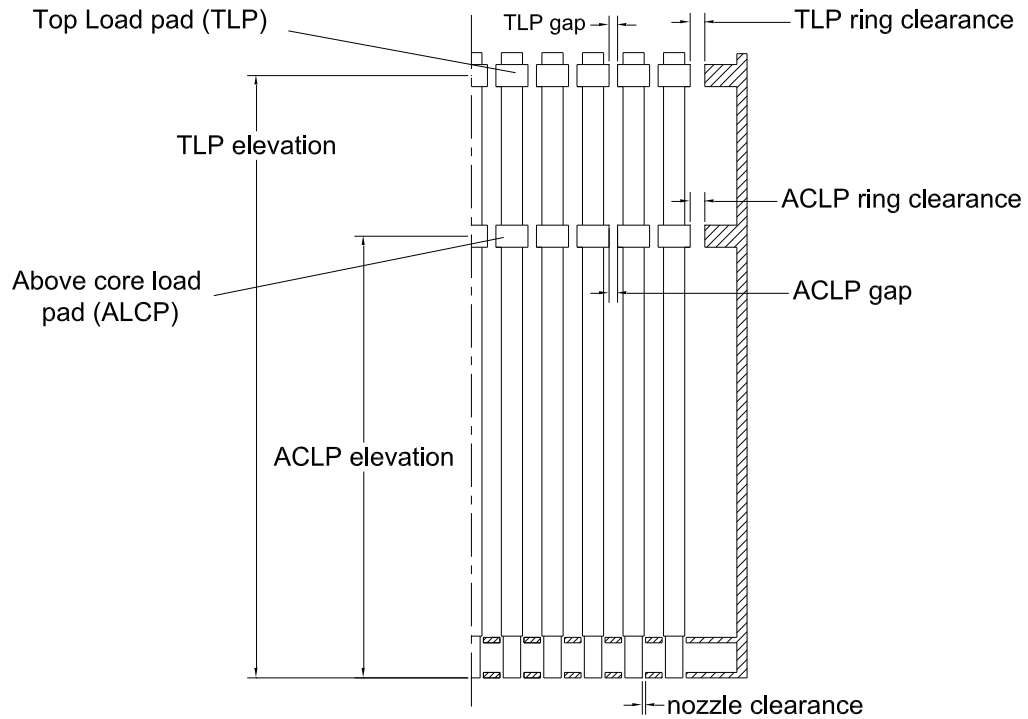


**Figure 5.5 Schematic of Limited Free Bow Core Restraint System Components and Key Dimensions.**

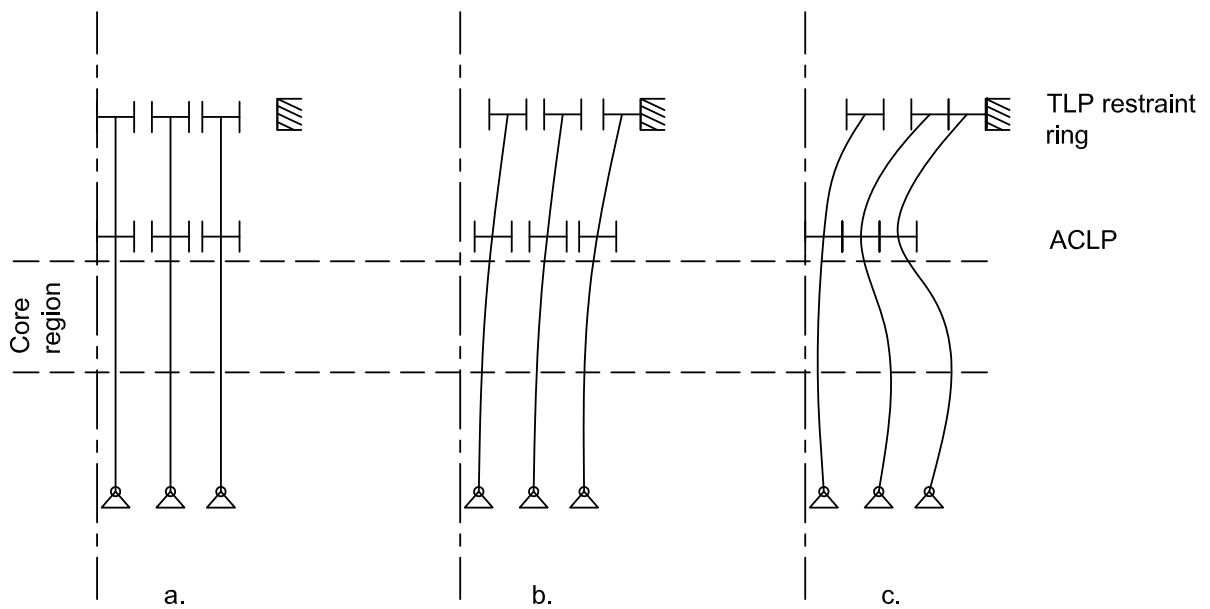


**Figure 5.6 Illustration of Limited Free Bow Core Restraint Concept.**

Figure 5.6a shows the nominal configuration of the ducts with no temperature gradient. As the radial thermal gradient develops (increasing temperature as distance from centerline decreases), the ducts begin to bow outward as shown in Figure 5.6b. Prior to contact with the top core restraint ring, the duct bends away from the core centerline as the temperature increases and therefore reduces the reactivity insertion. After contacting the top restraint ring and as the temperature gradient increases, the center of the duct bows inward which temporarily increases the reactivity. As the gradient increases, the inward bowing continues until the ducts contact at the ACLP. When the interior ducts all contact at the ACLP, the reactor is ‘locked-up’ and no further compaction can occur. Subsequent increased thermal gradients cause a reverse bowing below the ACLP moving the core region away from the core center as illustrated in Figure 5.6c. At this point the reactivity generally decreases with constant negative slope as temperature increases. The core restraint system is designed to have this lock-up occur below the nominal operating core outlet temperature.

## 5.2 Core Mechanical Geometry

The dimensions of the core restraint system at nominal room temperature (21°C) are listed in Table 5.1. The referenced dimensions are illustrated in Figure 5.7 through Figure 5.12. The fuel assembly duct dimensions are shown in Figure 5.7. The pitch, duct-duct gap and duct-load pad gap, illustrated in Figure 5.8, are temperature- and elevation- dependent. The restraint ring, core barrel and restraint system dimensions are shown in Figure 5.9 through Figure 5.13. The materials for the main components are listed in Table 5.2.

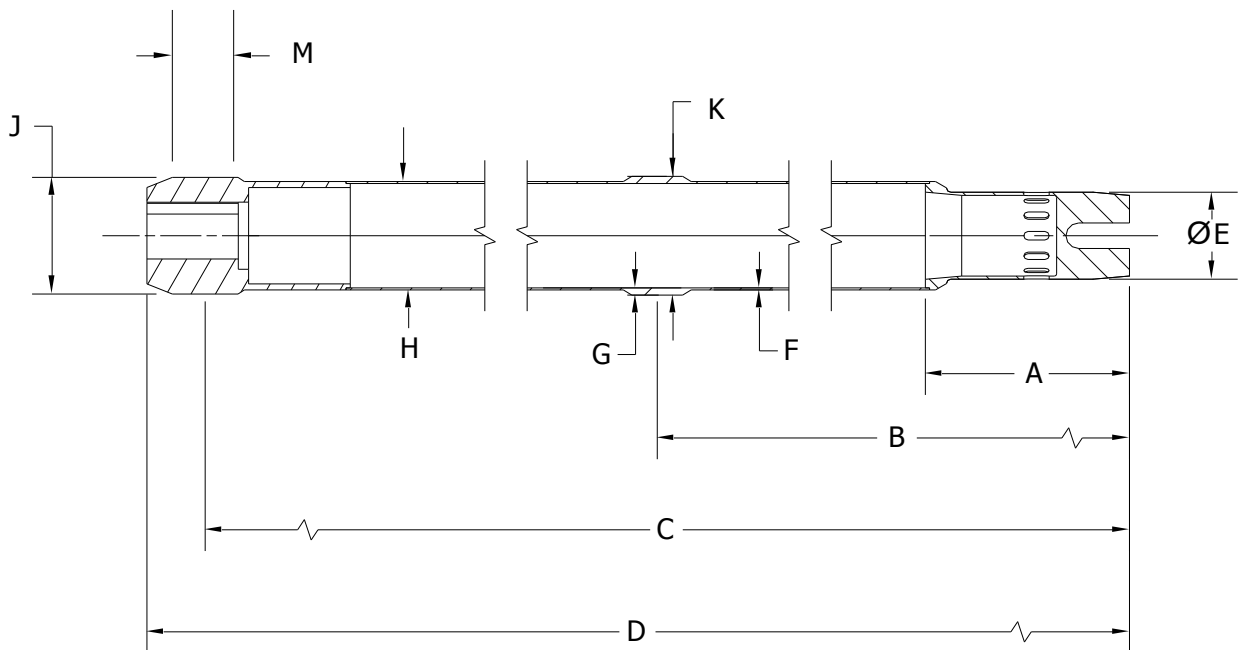


**Figure 5.7 Schematic for Duct Dimensions.**

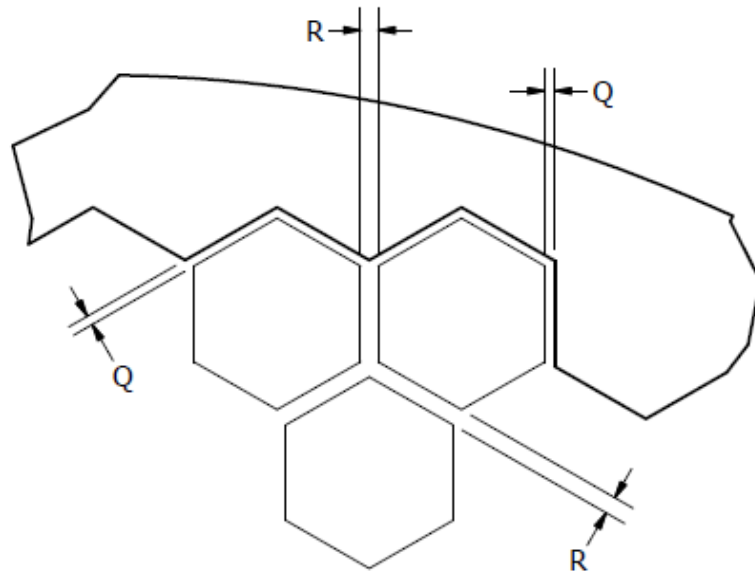


**Figure 5.8 Schematic of Restraint Ring Gap Dimensions at TLP which illustrates the Load Pad Gap (R) and the Load Pad-TLP Restraint Ring gap (Q).**

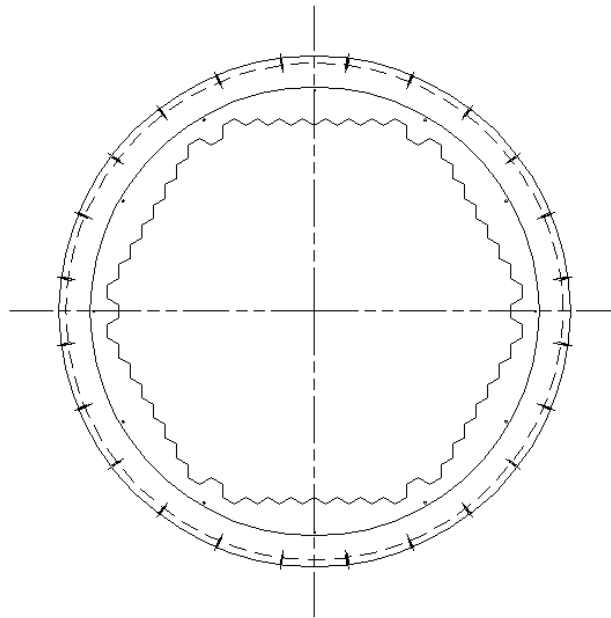


**Figure 5.9 Plan View of Typical Restraint Ring.**

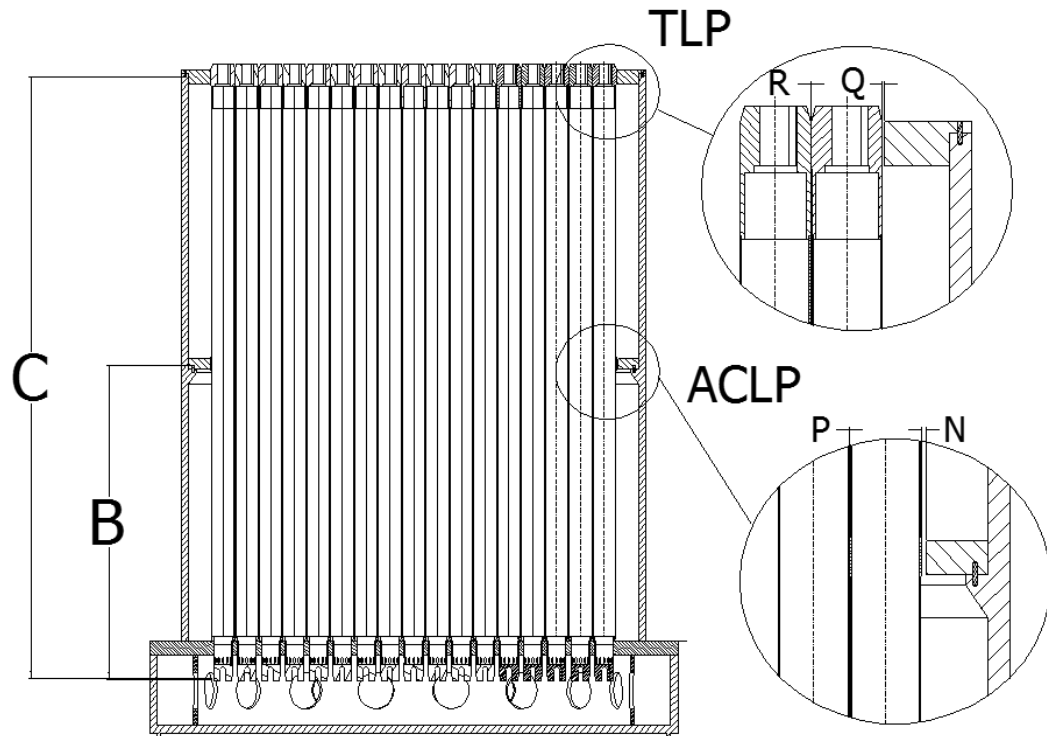


**Figure 5.10 Core Restraint Schematic for Dimensions Showing Top Load Pad (TLP) and Above Core Load Pad (ACLP).**

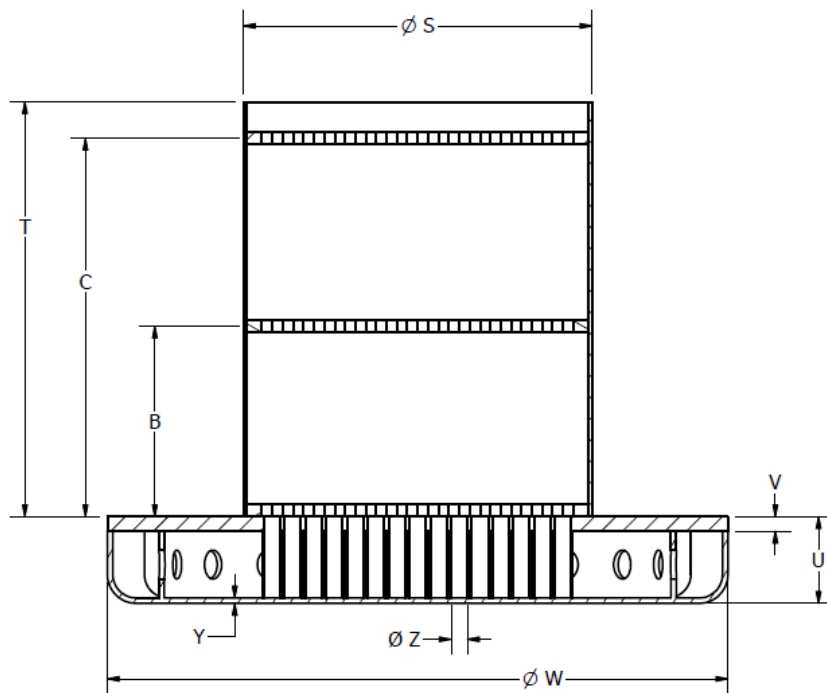


**Figure 5.11 Dimensions for Core Barrel.**

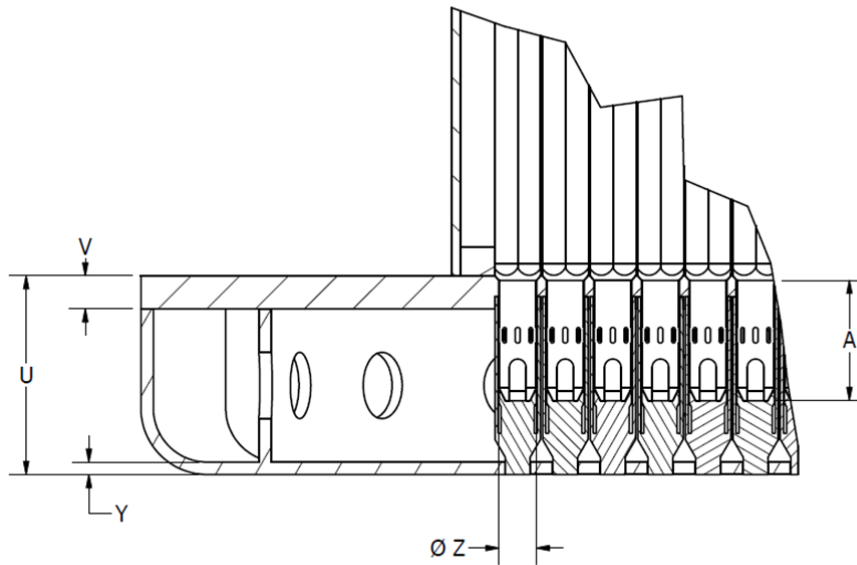


**Figure 5.12 Additional Detail of Duct Inlet Nozzle Connection to Inlet Receptacle.**

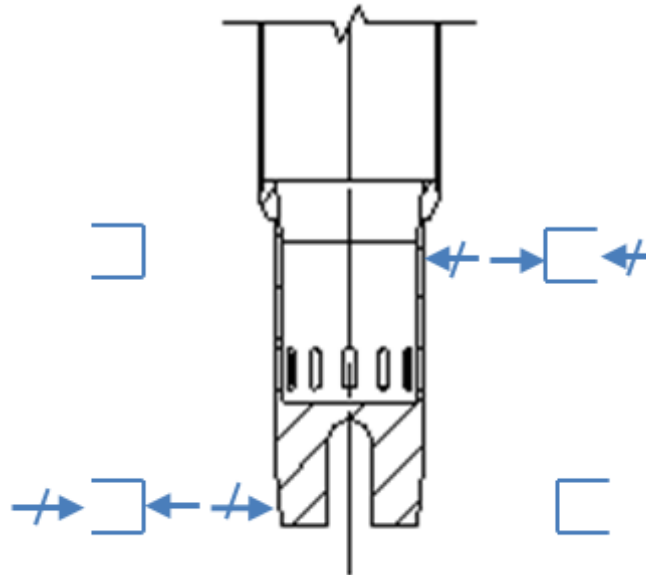


**Figure 5.13 Illustration of Duct Boundary Condition: Nozzle Laterally Restrained by Contact with Receptacle.**

Figure 5.13 illustrates the duct boundary condition assumption. The nozzle is laterally restrained by contact with the receptacle. The figure illustrates the duct leaning to one side and with exaggerated clearances. Note that clearance at top and bottom can be different.

**Table 5.1. Key Dimensions Related to the Core Restraint Design Shown in Figure 5.7 through Figure 5.12 (Evaluated at  $T_{ref} = 21^{\circ}\text{C}$ ).**

<i>Label</i>	<i>Description</i>	<i>Dimension</i>	
		<i>[in]</i>	<i>[cm]</i>
<b>A</b>	Nozzle length	15.0	38.0
<b>B</b>	ACLP elevation	74.1	188.2
<b>C</b>	TLP elevation	125.1	317.8
<b>D</b>	Duct length	129.1	328
<b>E</b>	Nozzle diameter	4.500	11.43
<b>F</b>	Duct wall thickness	0.118	0.3
<b>G</b>	ACLP wall thickness	0.170	0.43
	TLP wall thickness	0.170	0.43
<b>H</b>	Duct across the flats	5.590	14.20
<b>J</b>	TLP across the flat	5.694	14.463
<b>K</b>	ACLP across the flat	5.694	14.463
<b>M</b>	Load pad height	4	10.16
<b>N</b>	ACLP restraint-ring to load pad clearance at $T_{ref}$	0.5	1.27
<b>P</b>	ACLP load pad gap at $T_{ref}$	0.053	0.135
<b>Q</b>	TLP restraint-ring to load pad clearance at $T_{ref}$	0.036	0.091
<b>R</b>	TLP load pad gap at $T_{ref}$	0.053	0.135
<b>S</b>	Core barrel outer diameter	96.4	244.9
<b>T</b>	Core barrel height	114.84	291.7
<b>U</b>	Inlet plenum height	24.00	61
<b>V</b>	Grid plate thickness	4.00	10.16
<b>W</b>	Inlet Plenum Structure diameter	171.50	435.6
<b>Y</b>	Inlet Plenum structure thickness	1.5	3.81
<b>Z<sup>1</sup></b>	Upper nozzle receptacle diameter	4.510	11.46
<b>Z<sup>1</sup></b>	Lower nozzle receptacle diameter	4.510	11.46

<sup>1</sup>Note that the upper and lower nozzle receptacle clearances may be different as discussed in Figure 5.13. This dimension is identified by the single variable ‘Z’ in Figure 5.11 and Figure 5.12.

### 5.3 Structural Mechanical Material Properties

This section lists the structural mechanical properties of the various materials. The assembly duct is made of HT-9 whereas the grid plate, restraint rings, and core barrel are made of SS-316.

**Table 5.2 Component Materials**

Component	Material
Assembly duct	HT-9
Grid plate	SS-316
Restraint rings	SS-316
Core Barrel	SS-316

**Table 5.3 Mechanical Properties for HT-9.**

Property	Symbol	Relation (from Ref. 11)	Units
Instantaneous coefficient of thermal expansion	$\alpha(T)$	$9.2207 + (1.5161 \cdot 10^{-2})T - (1.0624 \cdot 10^{-5})T^2$ , $21 < T < 650$	$\alpha [10^{-6} / ^\circ\text{C}]$ , $T [^\circ\text{C}]$
Modulus of Elasticity	$E(T)$	$(213.28 - 4.799 \cdot 10^{-2}T - 4.065 \cdot 10^{-6} T^2) \cdot 10^3$	$E[\text{Mpa}]$ , $T [^\circ\text{F}]$
Poisson's ratio	$\nu$	$0.2762 + 8.9309 \cdot 10^{-5}T - 6.262 \cdot 10^{-8} T^2$	$T [^\circ\text{F}]$

**Table 5.4 Mechanical Properties for SS-316.**

Property	Symbol	Relation	Units	Ref.
Instantaneous coefficient of thermal expansion	$\alpha(T)$	$1.789 \cdot 10^{-5} + 2.398 \cdot 10^{-9}T - 3.269 \cdot 10^{-13} T^2$ , $400 < T < 1700$	$\alpha [10^5 / \text{K}]$ , $T [\text{K}]$	[12]
Modulus of Elasticity	$E(T)$	$200.7 - 7.3168 \cdot 10^{-2} T - 1.2719 \cdot 10^{-5} T^2$ , $25 < T < 649$	$E[\text{GPa}]$ , $T [^\circ\text{C}]$	Fit from data in [13]
Poisson's ratio	$\nu$	$0.2554 + 2.961 \cdot 10^{-4}T - 2.7362 \cdot 10^{-7} T^2$ , $25 < T < 649$	$T [^\circ\text{C}]$	Fit from data in [13]

## 6 Thermal Hydraulic Specification

### 6.1 Inlet and Outlet Temperatures

The assumed temperatures at operating condition are given in Table 6.1. The coolant inlet and bulk outlet temperatures are 355°C and 510°C, respectively [7]. The average flow rate was determined such that the coolant temperature rise across the core is 155°C. A chopped cosine shape was assumed for the axial power distribution.

**Table 6.1 Assumed Temperature at Operating Condition**

Temperature (°C)	Inlet Temperature	355.0
	Outlet Temperature	510.0
	Coolant in active core	432.5
	Cladding	462.5
	Fuel	582.5
	Reflector	432.5
	Shield	355.0
	Lower structure and reflector	355.0
	Upper plenum and structure	510.0

**6.2 Material Properties for T/H**

Some material properties including density, thermal conductivity, specific heat, and viscosity are given in Table 6.2.

**Table 6.2 Thermal Hydraulic Properties for Materials**

Material	Density	Thermal Conductivity	Viscosity
Sodium Coolant Ref. [12]	<i>Units: kg/m<sup>3</sup></i> <i>T in °C</i> $\rho = a + bT + cT^2 + dT^3$ $a = 950.1$ $b = -0.22976$ $c = -1.46 \cdot 10^{-5}$ $d = 5.64 \cdot 10^{-9}$	<i>Units: W/cm-K</i> <i>T in °C</i> $\kappa = a + bT + cT^2$ $a = 0.930$ $b = -0.581 \cdot 10^{-3}$ $c = 1.173 \cdot 10^{-7}$	<i>Units: Pa-s</i> <i>T in °K (Kelvin)</i> $\mu = 10^{(a+b/T+c \log_{10}(T))}$ $a = -2.487$ $b = 220.65$ $c = -0.4925$
HT-9 Clad and Duct [14]	<i>Units: g/cc</i> <i>T in °C (0 to 800)</i> $\rho = a + bT$ $a = 7.778$ $b = -3.07 \cdot 10^{-4}$	<i>Units: W/m-K</i> <i>T in °C</i> $\kappa = a + bT$ $a = 24.7608$ $b = 4.02 \cdot 10^{-3}$	<i>Not applicable</i>
SS-316 Structure Ref. [12]	<i>Units: g/cm<sup>3</sup></i> <i>T in °K (Kelvin)</i> $\rho = a + bT + cT^2$ $a = 8.084$ $b = -4.209 \cdot 10^{-4}$ $c = -3.894 \cdot 10^{-8}$	<i>Units: W/cm-K</i> <i>T in °K (Kelvin)</i> $\kappa = a + bT$ $a = 9.248 \cdot 10^{-2}$ $b = 1.571 \cdot 10^{-4}$	<i>Not applicable</i>

### 6.3 Core Subassembly Flow Allocation and Power

The core flow allocation, i.e. flow rate in each subassembly, is derived from information about the SAS4A/SASSYS-1 safety analysis performed in the ABTR Preconceptual Design Report (Section III.7.3 of Reference [7]). In the safety analysis, the active core assemblies were divided into five groups, based on considerations of flow and neutronics characteristics, with each group being modeled by a representative single-pin channel. Channels 1 (23 assemblies) and 3 represent the average subassemblies in the inner and outer enrichment zones, respectively, while channel 2 represents the average of the mid-core fuel test assemblies. A fourth channel represents all of the non-fuel subassemblies, including the mid-core materials test assemblies. Channel 5 is used to represent the peak-power inner-core subassembly with fresh fuel. The total core flow rate is 1264.4 kg/s at the hot operating condition. The allocation into the five groups of assemblies is shown in Table 6.3 and Figure 6.2.

**Table 6.3 Flow Allocation in Safety Analysis Model [7]**

Channel	Number of Pins	Number of Assemblies	Initial Subassembly Coolant Flow (kg/s)
1	217	23	23.33
2	217	6	20.81
3	217	30	18.42
4	91	81	0.297
5	217	1	26.35

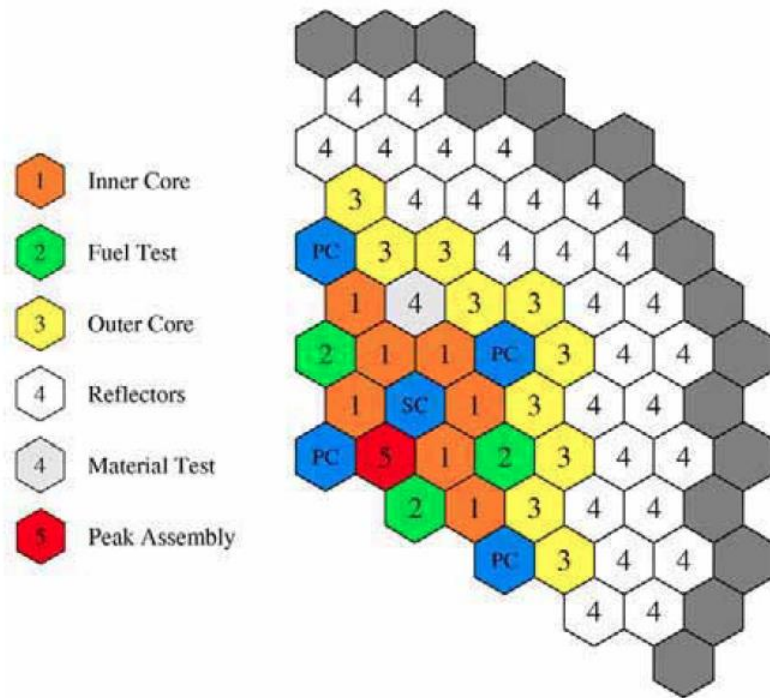


**Figure 6.1 Subchannel Assignments in Safety Analysis Model [7].**

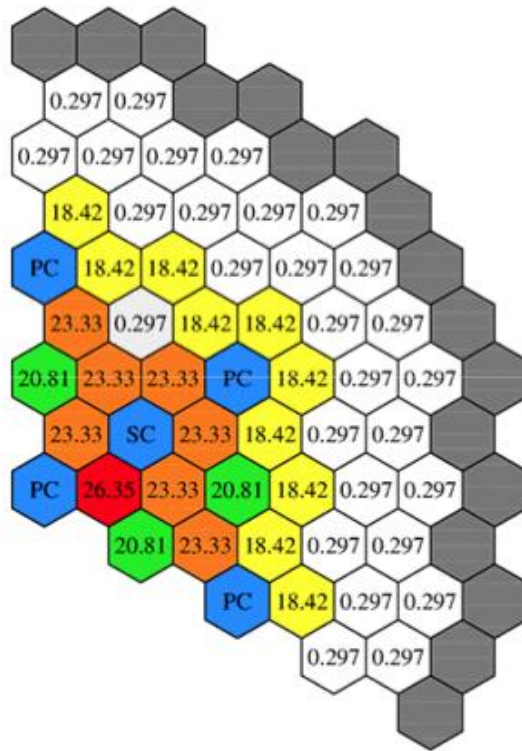


Figure 6.2 Initial Subassembly Flow Rate (kg/s) in Safety Analysis Model [7]

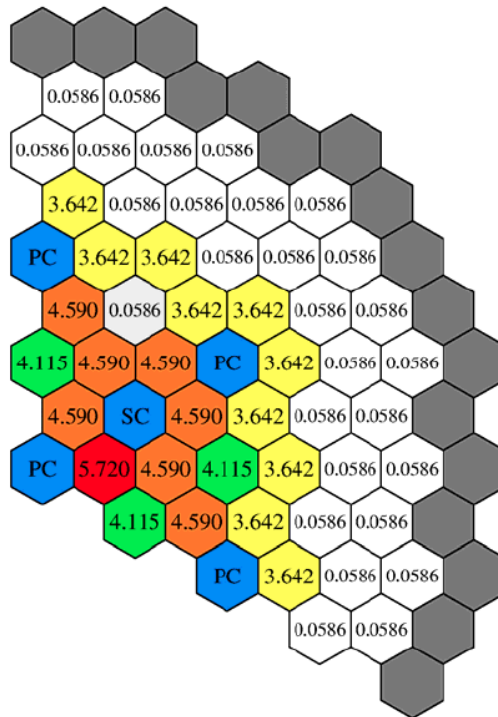


Figure 6.3 BOEC Subassembly Powers (MW) [7].

## 7 Kinetics Parameters

The radial expansion coefficient represents the reactivity effects of uniform, radial thermal expansion of the grid plate (SS-316) that is governed by the coolant inlet temperature. The axial expansion coefficient represents the reactivity effects of uniform, axial thermal expansion of fuel for the case that the fuel is bonded to the cladding.

**Table 7.1 Kinetics Parameters and Reactivity Coefficients (from Ref. [7])**

	Unit	BOEC	EOEC
Effective delayed neutron fraction $\beta$		0.0033	0.0033
Prompt neutron lifetime	$\mu s$	0.33	0.33
Radial expansion coefficient	cent/ $^{\circ}C$	-0.59	-0.60
Axial expansion coefficient	cent/ $^{\circ}C$	-0.06	-0.05
Fuel density coefficient	cent/ $^{\circ}C$	-0.75	-0.76
Structure density coefficient	cent/ $^{\circ}C$	0.03	0.03
Sodium void worth	\$	1.75	1.85
Sodium density coefficient	cent/ $^{\circ}C$	0.03	0.03
Doppler coefficient	cent/ $^{\circ}C$	-0.10	-0.10
Sodium voided Doppler coefficient	cent/ $^{\circ}C$	-0.07	-0.07

## References

1. A. Siegel, T. Tautges, A. Caceres, D. Kaushik, P. Fischer, G. Palmiotti, M. A. Smith, and J. Ragusa, "Software Design of SHARP," Proceedings of the Joint International Topical Meeting on Mathematics and Computations and Supercomputing in Nuclear Applications (M&C + SNA), American Nuclear Society, April 2007.
2. M. A. Smith, D. Kaushik, A. Wollaber, W. S. Yang, B. Smith, C. Rabiti, and G. Palmiotti, "Recent Research Progress on UNIC at Argonne National Laboratory," Proceedings of the International Conference on Mathematics, Computational Methods and Reactor Physics (M&C), American Nuclear Society, April 2009.
3. P. F. Fischer, J. W. Lottes, and S. G. Kerkemier, NEK5000 Web Page, <http://nek5000.mcs.anl.gov>, 2008.
4. D. Parsons, J. M. Solberg, R. M. Ferencz, M. A. Havstad, N. E. Hodge, and A. P. Wemhoff, "Diablo User Manual," UCRL-SM-234927, Lawrence Livermore National Laboratory, September 2007.
5. T. J. Tautges, R. Meyers, K. Merkley, C. Stimpson, and C. Ernst, "MOAB: A Mesh-Oriented Database," SAND2004-1592, Sandia National Laboratories, April 2004.
6. F. E. Dunn, T. H. Fanning, and J. E. Cahalan, "Preliminary Safety Evaluation of the Advanced Burner Test Reactor," ANL-AFCI-172, Argonne National Laboratory, September 15, 2006.
7. Y. I Chang, et al., "Advanced Burner Test Reactor Preconceptual Design Report," ANL-ABR-1 (ANL-AFCI-173), Argonne National Laboratory, September 5, 2006.
8. M. Tentner, "Severe Accident Approach – Final Report Evaluation of Design Measures for Severe Accident Prevention and Consequence Mitigation," ANL-GENIV-128, Argonne National Laboratory, March 2010.
9. A. Waltar and A. Reynolds, "Fast Breeder Reactors", Pergamon International Library, 1981.
10. R. A. Wigeland, and T. J. Moran, "Radial core expansion reactivity feedback in advanced LMRs: Uncertainties and their effects on inherent safety," *Proceedings of the International Topical Meeting on Safety of Next Generation Power Reactors*. Seattle, WA: American Nuclear Society, 1988.
11. S. Sharafat, R. Amodeo, and N. Ghoniem, "Materials Database and Design Equations for the UCLA Solid Breeder Blanket," UCLA-ENG-8611, February 1986.
12. L. Leibowitz, et al, "Properties for LMFBR Safety Analysis," ANL-CEN-RSD-76-1, Argonne National Laboratory, March 1976.
13. M. Grujicic and H. Zhao, "Optimization of 316 stainless steel:alumina functionally graded material for reduction of damage induced by thermal residual stresses," *Material and Science Engineering*, A252, pp. 117-132, 1998.
14. Unpublished Information, Argonne National Laboratory, November 1985.
15. K. L. Basehore and N. E. Todreas, "SUPERENERGY-2: A Multiassembly Steady-State Computer Code for LMFBR Core Thermal-Hydraulic Analysis," PNL-3379, Pacific Northwest Laboratory, August 1980.



## **Nuclear Engineering Division**

Argonne National Laboratory  
9700 South Cass Avenue, Bldg. 208  
Argonne, IL 60439

[www.anl.gov](http://www.anl.gov)



Argonne National Laboratory is a U.S. Department of Energy  
laboratory managed by UChicago Argonne, LLC